RSC Advances

Superhydrophobic modification of PVDF-SiO$_2$ electrospun nanofiber membranes for vacuum membrane distillation

Zhe-Qin Dong, Xiao-hua Ma, Zhen-Liang Xu*, Zhi-yun Gu

Electrospun nanofiber membranes having a hierarchical structure with multilevel roughness were generated via electrospinning of poly (vinylidene fluoride) (PVDF)-SiO$_2$ blend solutions. The composite PVDF-SiO$_2$ nanofiber membranes were then endowed with superhydrophobicity by the fluorosilanization of the surface with low surface energy fluoroalkylsilane (FAS). The results showed that when the SiO$_2$ content in the dope solutions increased from 0 wt% to 8 wt%, the water contact angles of the FAS modified nanofiber membranes increased significantly from 130.4° to 160.5°. The increment of the silica content in the dope solutions decreased the fiber diameters and pore sizes of the modified membranes, while the mechanical properties were enhanced with the silica addition. The liquid entry pressures of the membranes increased gradually from 84 kPa to 195 kPa with silica addition due to the increased contact angles and decreased pore size. Vacuum membrane distillation experiments were carried out for the modified nanofiber membranes to evaluate the anti-wetting properties. The optimal superhydrophobic nanofiber membrane maintained a stable flux of 31.5 kg/m^{2}h with a permeate conductivity approximately 10 μs/cm over the entire test, while the fluxes and conductivities of the nanofiber membranes without superhydrophobicity showed a significant decrease and increase, respectively. The results indicated that the superhydrophobic modification process rendered the nanofiber membrane anti-wetting properties without compromising its excellent permeability.

State Key Laboratory of Chemical Engineering, Membrane Science and Engineering R&D Lab, Chemical Engineering Research Center, Shanghai Key laboratory of Mutiphase Materials Chemical engineering, East China University of Science and Technology (ECUST), 130 Meilong Road, Shanghai 200237, China Email: chemxuzl@ecust.edu.cn; Tel: 86-21-64253061; Fax: 86-21-64252989.

1. Introduction

Membrane distillation (MD) is a non-isothermal separation process in which water vapor directly transports through a hydrophobic porous membrane under the partial gradient induced by the temperature difference between feed and permeate sides. There are generally four MD configurations, which include direct contact membrane distillation (DCMD), vacuum membrane distillation (VMD), air gap membrane distillation (AGMD), and sweep gas membrane distillation (SGMD). With the advantages of easy operation, low energy consumption and high salt rejection, MD is an attractive candidate for seawater desalination and water treatment.[1-4] However, the currently-used MD membranes are mainly fabricated by the conventional processes such as phase separation or stretching, unsatisfied permeability of the membranes caused by their low porosity and tortuous structure hampers the industrial implementation of MD processes.[5-6]

Recently, a considerable attention has been devoted to explore the feasibility and optimization of electrospun nanofiber membranes (ENMs) for application in MD. The results reveal that these ENMs exhibit several attractive features for MD process, such as high hydrophobicity, high porosity and inter-connected structure.[7-10] Unfortunately, the smooth ENMs prepared solely by hydrophobic polymers usually display strong water adhesion regardless of their high contact angles, which makes them susceptible to membrane wetting.[9] As a result, more steps are needed to prevent pore wetting issue in MD process.

Typically, the problem of pore wetting can be alleviated by two approaches, either increasing surface hydrophobicity or decreasing pore diameter.[11] Compared with decreasing membrane pore diameter, increasing surface hydrophobicity is a preferable way to alleviate pore wetting, as reduced pore size would likely result in lower permeability. Therefore, superhydrophobic membranes are desirable in MD process for possessing the nonwettable properties.[12] Based on the model of Cassie–Baxter, an air gap is introduced between the water drop and the superhydrophobic surface, which increases the allowable pore size of the membrane and improves the permeate flux.[13-14]

Fundamentally, the hydrophobicity of a solid surface lies on its surface energy and

geometrical structure.[15] Consequently, there are two ways to achieve superhydrophobic surfaces: (1) creating a rough surface on hydrophobic materials, and (2) modifying a rough surface with a low surface energy material. A number of strategies have been reported under this guidance, such as sol-gel process,[16-17] plasma etching,[18] chemical vapor deposition,[19] self-assemble,[20] electrospinning,[21-22] template synthesis,[23] and phase separation.[24] It is recognized that utilization of nanoparticles is an effective way for the preparation of superhydrophobic surface in recent studies.[25-27] Superhydrophobic membranes for MD were fabricated by Zhang et al. via spraying a mixture of polydimethylsiloxane (PDMS) and hydrophobic SiO_2 nanoparticles on poly (vinylidene fluoride) (PVDF) flat sheet membranes.[25] Privett et al. synthesized a superhydrophobic xerogel coating with a mixture of nanostructured fluorinated silica colloids, fluoroalkoxysilanes, and a backbone silane, which exhibited an excellent anti-fouling property.[26] Razmjou et al. prepared a superhydrophobic membrane via TiO_2 coating by a low temperature hydrothermal (LTH) process followed by the fluorosilanization of the surface with fluoroalkylsilane (FAS).[27] However, utilizing nanoparticles to prepare superhydrophobic ENMs for MD process has rarely been reported.

Herein, we describe a new strategy to prepare superhydrophobic membranes with remarkable permeability and desirable anti-wetting properties for MD process. As SiO_2 nanoparticles exhibited improved performance and good compatibility in the preparation of PVDF nanocomposite membranee,[28-29] the superhydrophobic nanofiber membranes were generated by a two-step approach. Firstly, PVDF-SiO_2 nanofiber membranes with a hierarchical structure were obtained by eletrospinning of PVDF-SiO_2 blend solutions. Then, the as-spun PVDF-SiO_2 nanofiber membranes were immersed into a FAS solution to reduce the surface energy and improve the surface hydrophobictiy. The prepared membranes were characterized in terms of scanning electron microscopy (SEM), X-ray photoelectron spectroscopy analysis (XPS), atomic force microscopy (AFM), water contact angles (WCAs), liquid entry pressure of water (LEPw) values and mechanical properties to investigate their surface and structure. Finally, vacuum membrane distillation experiments were carried out for the FAS-modified PVDF-SiO_2 nanofiber membranes to evaluate the anti-wetting performance.

2. Experimental

2.1. Materials

PVDF (Solef® 6010) was purchased from Solvay Advanced Polymers, L.L.C (Alpharetta GA, USA) and SiO_2 nanoparticles (20-50 nm) were purchased from Zhejiang Hongsheng CO. LTD (China). (Heptadecafluoro-1,1,2,2-tetradecyl) trimethoxysilane (FAS-17) was obtained from Nanjing Chengong Organic Silica Materials CO. LTD (China). All other solvents and reagents were analytical grade and purchased from Shanghai Sinopharm Chemical Reagent CO. LTD (China). A Commercial polytetrafluoroethylene (PTFE) membrane manufactured by Sumitomo Electric Industries CO. LTD was used to compare with the FAS-modified nanofiber membranes in vacuum membrane distillation. The Commercial PTFE membrane is denoted as S0.

2.2. Preparation of PVDF-SiO_2 electrospun nanofiber membranes

Firstly, PVDF was dissolved in a solvent mixture of dimethylacetamide (DMAC) and acetone (1:1 wt %) at a concentration of 15 wt %. The polymer solution was magnetically stirred for 24 h at room temperature to form a homogeneous solution, then different amounts of silica nanoparticles (0, 2, 4, 8 wt %) were added into the polymer solution. Finally, the PVDF-silica dope solutions were ultrasonic treated for 4 h to ensure the well-distribution of the silica nanoparticles. The compositions of the dope solutions are listed in Table 1.

Table 1 Compositions of electrospinning dope solutions

Sample	PVDF (wt %)	SiO_2 (wt %)	DMAC (wt %)	Acetone (wt %)
S1	15	0	42.5	42.5
S2	15	2	41.5	41.5
S3	15	4	40.5	40.5
S4	15	8	38.5	38.5

The PVDF-SiO_2 dope solutions were electrospun under the following condition: the eletrospun rate was 2 ml/h, and the applied voltage was 18 kV across a distance of 15 cm, while the humidity and temperature were controlled at 50±5% and 25±1 ^{o}C, respectively. The electrospinning setup used in the present work was the same in our previous study.[30-33] The

4

as-pun PVDF-SiO$_2$ nanofiber membranes were then dried in an vacuum oven at 60 ^{o}C for 24 h to ensure the evaporation of the solvents.

2.3. Membrane modification

The PVDF-SiO$_2$ nanofiber membranes were immersed into a hexane solution with a FAS concentration of 2% for 24 h. These membranes are labeled as FAS-PVDF-SiO$_2$ nanofiber membranes. The schematic diagram for the superhydrophobic modification of PVDF-SiO$_2$ nanofiber membranes is shown in Fig. 1. Grafting occurs with a succession of condensation reactions between the OH groups found in the SiO$_2$ nanoparticles and the Si-O-alkyl groups of the silane. After modification, the samples were rinsed by hexane to remove the FAS remained at the membrane surface and heated at 100 ^{o}C for 12 h for the solvents to evaporate.
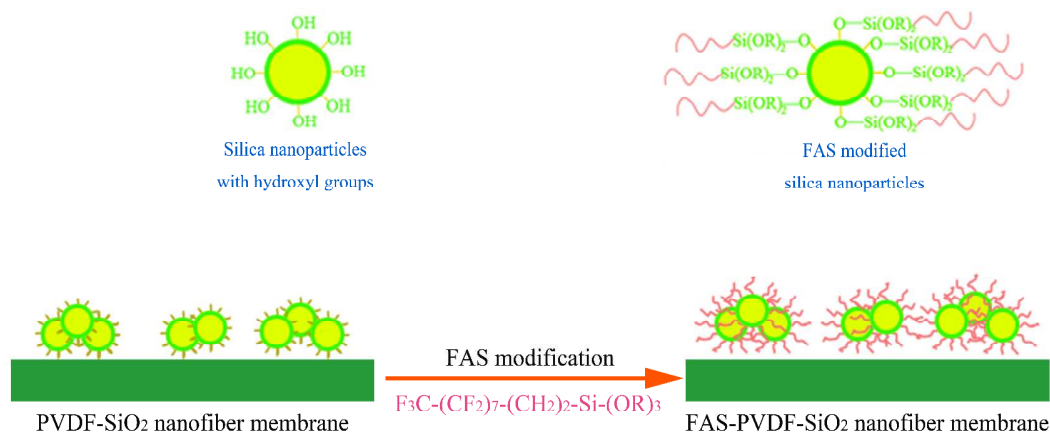

Fig. 1 Schematic diagram for the superhydrophobic modification of PVDF-SiO$_2$ nanofiber membranes

2.4. Membrane characterization

The morphologies of the FAS-PVDF-SiO$_2$ nanofiber membranes were observed by SEM (JSM-6360LV, Japan). The average fiber diameter was measured from the SEM images using J MicroVision image analyzer.

An XPS analysis (VG-miclabII, UK) was utilized to analyze the chemical composition on membrane surface precisely. Binding energies were calibrated with respect to C 1s hydrocarbon bond at 284.6eV.

Quantitative surface roughness analysis of the membranes was measured using AFM (Veeco, Nanoscope IIIa Multimode). Air-dried membrane sample was fixed on a specimen holder and 5μm×5μm areas were scanned with a resolution of 256 × 256 points.

The water contact angles were measured by a JC2000D1 (produced by Shanghai Zhongcheng Digital Technology Apparatus Co. Ltd., China) system. The water sliding angles were also measured by placing a 10 μl water drop on a horizontal membrane surface. The membrane was then inclined till the drop started to roll off from the surface.

The mean pore size and pore size distribution of the membranes were measured by a capillary flow porometer (model 3H-2000PB, produced by Beijing Beiside Technology Apparatus Co. Ltd., China). Its working principle is based on the bubble-point and gas permeation tests.

The maximum pore size of the membranes was characterized by the bubble pressure test reported in literature.[34] The bubble point pressure was determined by using a DJ-5 membrane bubble point testing instrument produced by Shanghai Eling filter equipment Co. Ltd. (China). A membrane was immersed in ethanol for at least 3 h and was fitted on the testing instrument. Next, the bubble point pressure was obtained automatically. The maximum pore size can be calculated by Laplace's equation: [35]

$$r_{max} = \frac{2\sigma\cos\theta}{P} \tag{1}$$

where σ is the surface tension of ethanol (22.8×10^{-3} Nm^{-1}), θ is the contact angle of ethanol to membrane(°), and P is the minimum bubble point pressure (MPa).

The membrane porosity is determined by gravity method reported elsewhere.[36]

The mechanical properties of the FAS-PVDF-SiO$_2$ nanofibrous membranes were tested by a universal testing machine (QJ210A, China) with a common used cross-head speed of 10 mm/min at room temperature.

The LEPw values were measured using a dead-end filtration set-up which was designed according to the method described by Smolder and Franken.[37] The dry hydrophobic membrane was placed in a dead end cell and the cell was topped up with DI water. Compressed nitrogen was used to apply pressure in the cell. The pressure was noted when the first drop of water came from the cell.

2.5. VMD performance test

The performances of the prepared nanofiber membranes and the commercial PTFE membrane were tested in a VMD setup, as shown in Fig. 2. On the feed side, the feed solution was circulated by a pump and a thermostatic bath was utilized to control the temperature of the feed solution. Deionized water was added into the feed tank every 15 min to maintain the concentration of the feed solution, and the quantity of the water was determined by the decrement weight of the feed tank measured by an electronic balance. The permeate vapor flux was condensed at the permeate side by a glass condenser with a refrigerating machine. The permeate pressure was measured by a mercurial pressure gauge, and the permeate flux was calculated by measuring the volume of the condensed water. All the experiments were carried out using the 3.5 wt% NaCl solution as a feed. The feed temperature and the permeate pressure were controlled at 333 K and 9 kPa, while the feed flow rate was kept at 90 L/h.
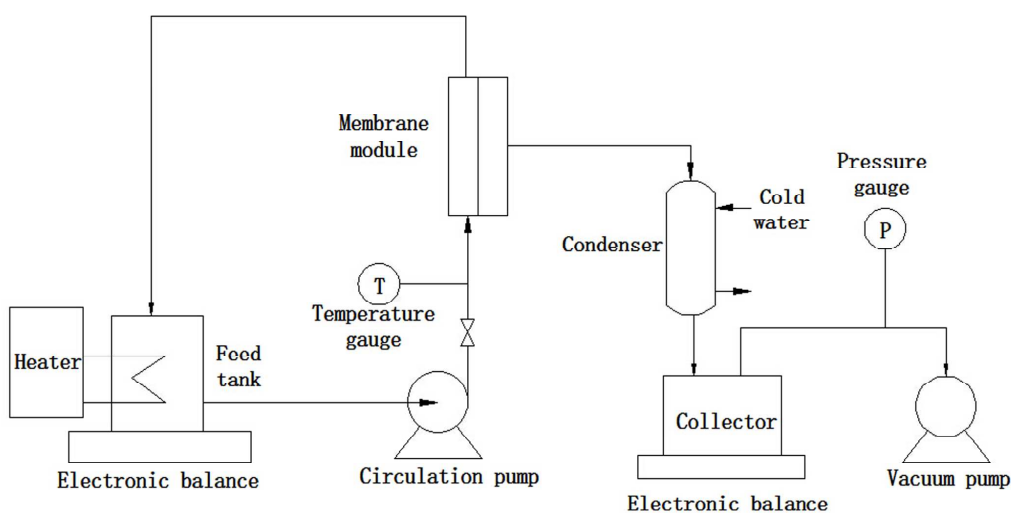

Fig. 2 Schematic diagram of vacuum membrane distillation

3. Results and discussions

3.1. Chemical modification reactions on PVDF-SiO$_2$ nanofiber membranes.

To investigate the effect of FAS modification on the surfaces of these nanofiber membranes, XPS measurements were conducted to analyze the surface chemical compositions of the

pristine PVDF nanofiber membrane, as-spun PVDF-SiO$_2$ nanofiber membrane and FAS-PVDF-SiO$_2$ nanofiber membrane with 8% silica loading, and the results were summarized in Fig. 3 and Table 2. It is clearly in Fig. 3 that the scan spectrum of the pristine PVDF nanofiber membrane only contains the C1s and F1s peaks. New O2s and Si2p peaks appear in the scan spectrums of PVDF-SiO$_2$ nanofiber membranes, which indicates the successfully deposition of SiO$_2$ on the outer surfaces of PVDF nanofibers since the probing depth of the XPS technique is less than 10 nm for this equipment. It is also illustrated in Table 2 that the percentage of Si element on the surface increases significantly from 0% to 5.07% with a silica loading of 8%, suggesting the sufficient amounts of silica nanoparticles on the outer surface. The deposited SiO$_2$ nanoparticles not only tailor the surface architecture of these nanofiber membranes, but also provide abundant OH groups for fluorosilanization. It is observed that the FAS modification has a notable effect on the surface chemical compositions of the PVDF-SiO$_2$ nanofiber membrane (Table 2). The percentage of F element increases significantly from 40.39% to 49% while the percentages of O and Si elements show an observable reduction after the FAS modification. The Si and O elements only account for 4.59% and 7.87% respectively in the FAS molecular (C$_{16}$H$_{19}$F$_{17}$O$_3$Si), which is much lower than those in SiO$_2$ nanoparticles (46.7% and 53.3%, respectively). Therefore, the percentages of O and Si elements on the surface decrease after the condensation reaction between deposited SiO$_2$ and FAS as illustrated in Fig. 1 .These XPS results confirm the self-assembled monomolecular layer of organosilane compound on the membrane surface.

Table 2 Elemental compositions of pristine PVDF nanofiber membrane, as-spun PVDF-SiO$_2$ nanofiber membrane and FAS-PVDF-SiO$_2$ nanofiber membrane

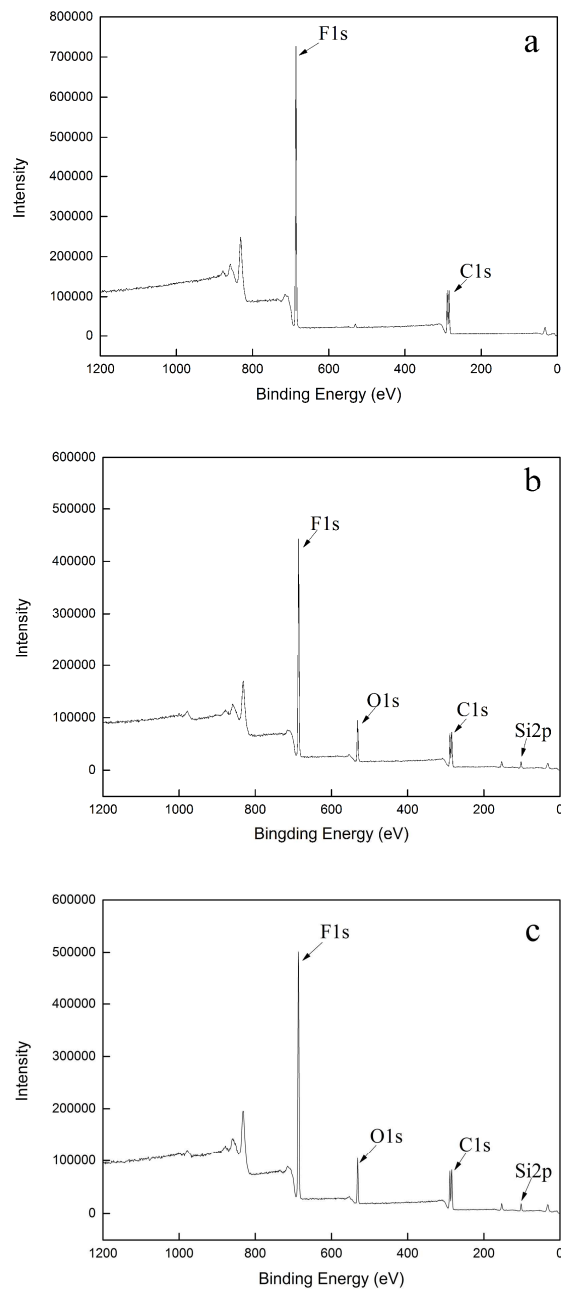| Sample	Atom percent (%)			
	C1s	O1s	F1s	Si2p
pristine PVDF	48.58	1.33	50.17	0.00
PVDF-SiO$_2$	43.64	10.91	40.39	5.07
FAS-PVDF-SiO$_2$	39.77	7.19	49.00	4.05

Fig. 3 XPS wide-scan of (a) pristine PVDF nanofiber membrane, (b) as-spun PVDF-SiO$_2$

nanofiber membrane and (c) FAS-PVDF-SiO$_2$ nanofiber membrane

3.2. Membrane morphology analysis

Fig. 4 presents the SEM images of the pristine PVDF nanofiber membrane and FAS-PVDF-SiO$_2$

nanofiber membranes with various SiO$_2$ contents. It is observed that the surfaces of the

pristine PVDF nanofiber membrane (a) and the FAS-modified membrane without SiO$_2$

addition (b) are both smooth and uniform. This indicates that direct grafting with FAS does

not have obvious effects on the surface morphology, concurring with the reports by previous researchers.[38-39] On the contrary, the rough particles appear on the surface of the membranes when SiO_2 nanoparticles are electrospun with PVDF (c-f), which indicates the depositions of SiO_2 nanoparticles on the PVDF nanofibers. Besides, with the increase of the silica content in the dope solutions, the amounts of rough particles increase significantly on the membrane surface. The aggregations of the SiO_2 nanoparticles are also observed in the SEM images due to the strong interaction between these nanoparticles. The effects of these aggregated SiO_2 nanoparticles on membrane hydrophobicity and permeability are discussed in details in the following sections.
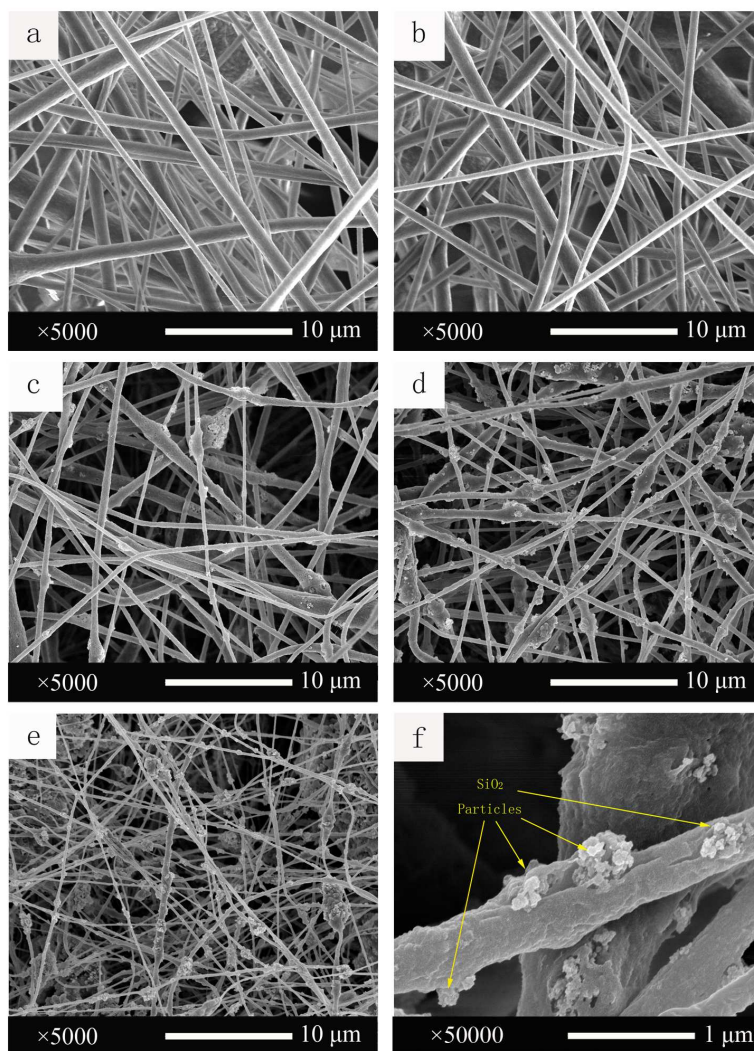

Fig. 4 Surface morphologies of (a) pristine PVDF nanofiber membrane; (b-e) FAS-PVDF-SiO_2 nanofiber membrane S1-S4 and (f) high magnification of S4

The fiber diameter distributions of the FAS-PVDF-SiO$_2$ nanofiber membranes with various SiO$_2$ contents were determined from the SEM image and the results are shown in Fig. 5. The results reveal that with the increase of silica content from 0 wt% to 8 wt% in the dope solutions, the average fiber diameters of the membranes decrease from 620 nm to 340 nm. This phenomenon can be explained as follows. The additions of silica nanoparticles limit the relative movement between the matrix molecule chains and thus reduce the elastic properties. Therefore, the die-swell ratio of the blend solutions decreases with the silica content, which results in the reduction of the fiber diameter. Similar investigations of nanoparticles addition on die-swell ratio have been conducted previously.[40-41]
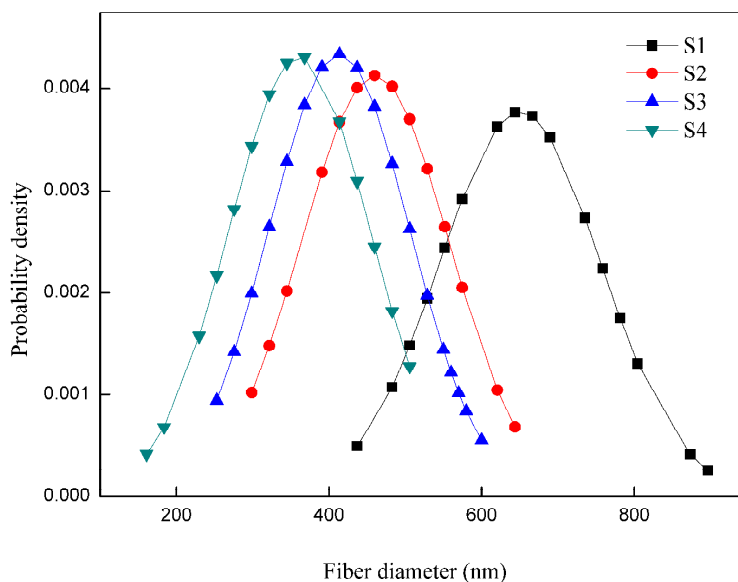

Fig. 5 Fiber diameter distributions of FAS-PVDF-SiO$_2$ nanofiber membranes with various SiO$_2$ contents

3.3. Membrane surface analysis

The water contact angles and sliding angles of the FAS-PVDF-SiO$_2$ nanofiber membranes as well as the water drops on membrane surface are summarized in Table 3 and Fig. 6. The results suggest that the increase of SiO$_2$ content has significant effects on the water repellence of these FAS-PVDF-SiO$_2$ nanofiber membranes. With the concentration of silica nanoparticles increasing from 0 wt% to 8 wt%, the water contact angles of the FAS-PVDF-SiO$_2$

nanofiber membranes increase sharply from 130.4° to 160.5° while the sliding angles decrease from 47° to 8°.

Table 3 water contact angles and sliding angles of FAS-PVDF-SiO$_2$ nanofiber membranes with various SiO$_2$ contents

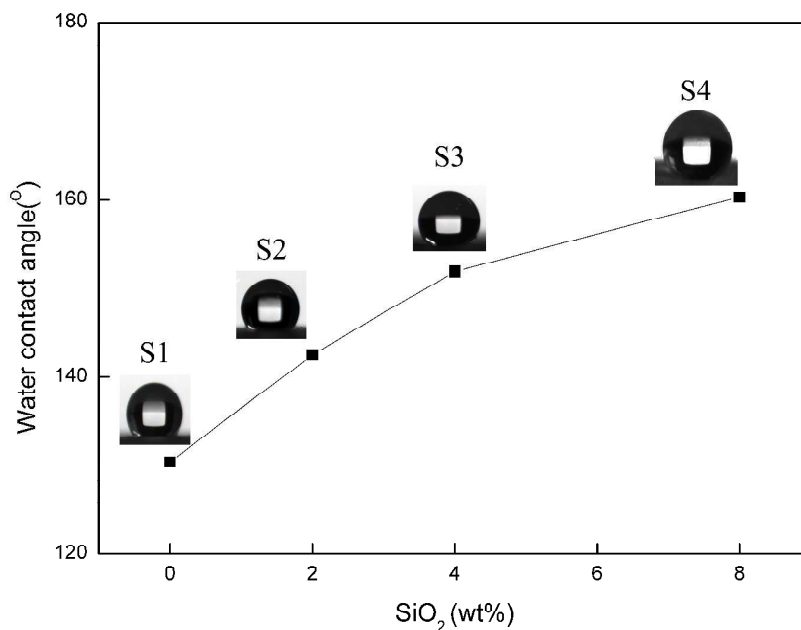| Sample	SiO2 loading (wt %)	Water contact angle (°)	Water sliding angle (°)
S1	0	130.4±1.5	47±5
S2	2	142.5±1.9	27±3
S3	4	151.9±2.0	11±2
S4	8	160.5±2.3	8±1

Fig. 6 Water drops on FAS-PVDF-SiO$_2$ nanofiber membranes with various SiO$_2$ contents

As is well known, the Young equation [35] gives the calculation method of the water contact angle for a flat surface as follows:

$$\cos \theta_0 = \frac{\gamma_{SA} - \gamma_{SL}}{\gamma_{LA}} \tag{2}$$

The characteristic angle ϑ_0 is called the static contact angle. γ_{SA} and γ_{SL} are the

surface energies of solid against air and liquid, respectively, and γ_{LA} is the surface energy of liquid against air.[41] Moreover, if a water droplet is placed on a rough surface with a homogeneous interface, the water contact angle can be obtained by the Wenzel equation: [42]

$$\cos\theta_w = R_f \cos\theta_0 \tag{3}$$

Where θ_w is the contact angle of a water droplet upon a rough solid surface calculated by Wenzel equation. R_f is the non-dimensional surface factor, equal to the ratio of the surface area to its flat projected area. It can be seen from the Wenzel model that the water contact angle of a hydrophobic surface ($\theta_0 > 90^\circ$) increases with the increase of surface roughness (R_f).

The depositions of SiO_2 nanoparticles on the PVDF nanofibers increase the surface roughness R_f of the nanofiber membranes as shown in the AFM images (Fig. 7). It could be observed that when the SiO_2 content increases from 0 wt% to 8 wt% in dope solutions, the average surface roughness (Ra) of the FAS-PVDF-SiO_2 nanofiber membranes increases significantly from 92 nm to 218 nm. Additionally, compared with the as-spun PVDF-SiO_2 nanofiber membranes, the FAS modification increases the percentage of F and decreases the percentage of O on the membrane surface as the XPS results indicated previously, thus reducing the surface energy γ_{SL} of the membrane surface. Considering the synergistic effect of the increased surface roughness R_f and reduced surface energy γ_{SL} of the FAS-modified membranes, the significant increase of the water contact angles is unsurprisingly according to equation (2)~(3). Moreover, the increased surface roughness reduces the total area of solid–liquid interface and increases the presence of air pockets on the membrane surface, which makes the water drops move easily and therefore decreases the water sliding angles.
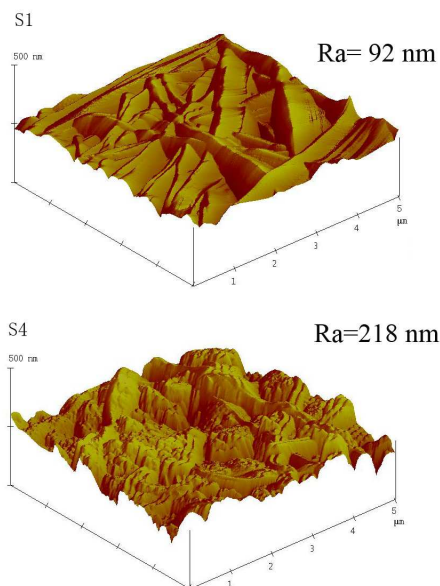
Fig. 7 AFM images of surface for FAS-PVDF-SiO$_2$ nanofiber membranes S1 and S4

3.4. Porosity, pore size, LEPw and mechanical properties

The common characteristics of the FAS-PVDF-SiO$_2$ nanofiber membranes and the commercial PTFE membrane are shown in Table. 4. It could be observed that all the FAS modified nanofiber membranes (S1-S4) possess a relative high porosity (77-83%) compared with commercial MD membrane S0 (55%), indicating that the FAS-modified membranes still have a porous open-connected structure after the surface modification. The porosity of these membranes decreases slightly with the increase of SiO$_2$ content, which is associated with the SiO$_2$ nanoparticles encased in the nanofibers. It can also be seen that the max pore size and mean pore size of these membranes decreases gradually by changing the SiO$_2$ content from 0 wt% to 8 wt%, which might be attributed to the decrease of fiber diameter and the aggregation of SiO$_2$ nanoparticles. Besides, the addition of SiO$_2$ nanoparticles narrows the pore size distribution of the nanofiber membranes (Fig. 8). As illustrated in Fig. 5, the silica addition renders the nanofiber membranes a better fiber diameter distribution and therefore leads to a narrower pore size distribution.

Table 4 Properties of FAS-PVDF-SiO$_2$ nanofiber membranes and commercial PTFE membrane

Sample	SiO$_2$ loading (wt%)	Fiber diameter (nm)	Membrane thickness (µm)	Mean pore size (µm)	Max pore Size (µm)	Porosity (%)	WCA (°)	LEPw (kPa)
S0			81±1	0.22±0.02	0.25±0.02	55±0.5	121.5±1.0	151±2
S1	0	620±160	102±5	0.38±0.03	0.45±0.03	83±1.5	130.4±1.5	84±2
S2	2	460±130	103±4	0.34±0.03	0.38±0.02	80±2.0	142.5±1.9	115±3
S3	4	390±115	98±3	0.29±0.02	0.34±0.02	79±2.0	151.9±2.0	145±3
S4	8	340±90	99±4	0.26±0.02	0.28±0.02	77±1.5	160.5±2.3	195±5
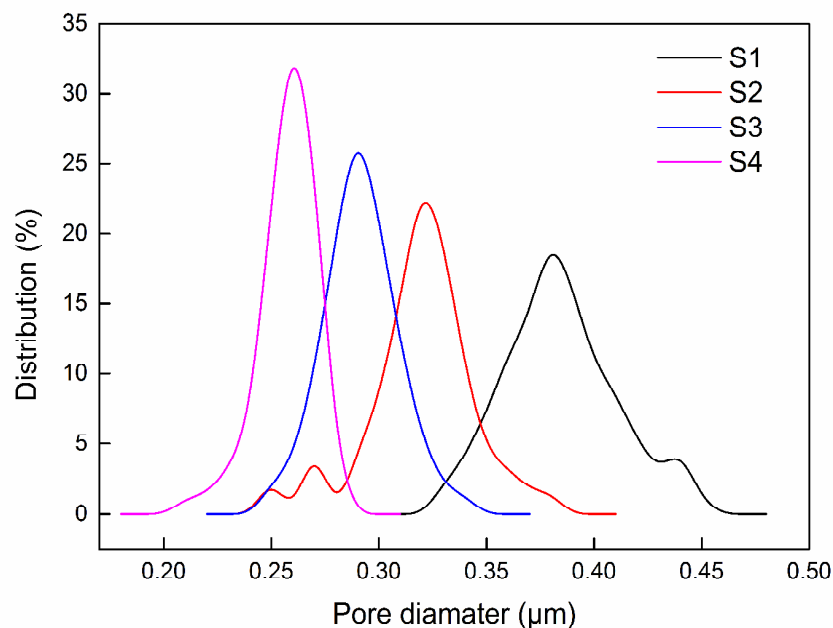
Fig. 8 Pore size distributions of FAS-PVDF-SiO$_2$ nanofiber membranes with various SiO$_2$ contents

To evaluate the wetting resistance of these membranes, the LEPw measurements were carried out. The results show that when the content of SiO$_2$ nanoparticles in the dope solutions varies from 0 wt% to 8 wt%, the LEPw values of the FAS-PVDF-SiO$_2$ nanofiber membranes increase remarkably from 84 kPa to 195 kPa (Table 4). The significant increase of the LEPw values with increasing SiO$_2$ loading can be explained as follows:

The LEPw value, which mainly depends on the pore size and membrane hydrophobicity can be obtained by the Laplace equation:

$$LEPw > \Delta P_{\mathrm{int}\,erface} = P_{liquid} - P_{vapor} = \frac{-2B\sigma\cos\theta}{r_{\max}} \qquad (4)$$

where B is a geometric factor determined by the pore structure, σ is the surface tension of the liquid (here, water) and θ is the contact angle of water to membrane.

As the increase of SiO_2 content increases the contact angle ϑ and decreases the max pore size r_{max} of the FAS-PVDF-SiO_2 membranes, the increase of LEPw value is expected according to equation (4). Besides, the LEPw value of the FAS-PVDF-SiO_2 nanofiber membrane with 8 wt% SiO_2 loading (195 kPa) is quite competitive, while the nanofiber membranes reported in previous studies only possessed a LEPw value around100 kPa.[7]

Based on the strain–stress measurements of the FAS-PVDF-SiO_2 nanofiber membranes, tensile strength, Young's modulus and elongation at break are tabulated in Table 5. It is obvious from the results that the mechanical properties of these membranes are improved with the increasing silica content. As the silica content increases from 0 wt% to 8 wt%, the tensile strength increases from 1.24 MPa to 2.24 MPa and the Young's modulus increases from 1.88 MPa to 3.20 MPa. The improvement could be attributed to the reduced porosity of nanocomposite membranes, which leads to a higher density of the polymer in the membranes. Besides, the silica nanoparticles could act as a crosslinking point in the composite membranes, which increases the rigidity of the polymeric chains and results in the improved mechanical performance.[43-45] However, the elongation at break is reduced with the silica addition, which implies the brittleness of the polymer-nanoparticle bonds.[45]

Table 5 Mechanical properties of FAS-PVDF-SiO_2 nanofiber membranes

Sample	SiO_2 loading (wt %)	Tensile Strength (MPa)	Young's Modulus (MPa)	Elongation at break (%)
S1	0	1.24±0.04	1.88±0.05	149±10
S2	2	1.58±0.05	2.45±0.08	140±8
S3	4	1.95±0.05	2.74±0.12	138±8
S4	8	2.24±0.07	3.20±0.15	128±5

3.5. Vacuum membrane distillation performance

As mentioned previously, membrane wetting is still a challenging issue for the electrospun

16

nanofiber membranes despite possessing high hydrophobicity.[9] It is expected that the superhydrophobictiy of FAS-PVDF-SiO$_2$ nanofiber membrane would alleviate the membrane wetting issue and maintain a stable performance. Therefore, vaccum membrane distillation experiments were carried out to test the permeability and anti-wetting performance of the surface modified nanofiber membranes.

The vacuum membrane distillation experiments were carried out with a 3.5 wt% NaCl solution and the results were shown in Fig. 9. It can be observed from Fig. 9 that the initial permeate fluxes of the modified nanofiber membranes S1-S4 were approximately 30 kg/m^{2}h, while that of the commercial PTFE membrane S0 was only 15 kg/m^{2}h under the same condition. Compared with the commercial PTFE membrane, the nanofiber membranes fabricated by electrospinning possessed a high porosity with open-connected structure, which resulted in the improvement of the permeate flux. The nanofiber membranes displayed a relative higher porosity of around 80%, while the commercial PTFE membrane only had a porosity of 55% (Table 4).
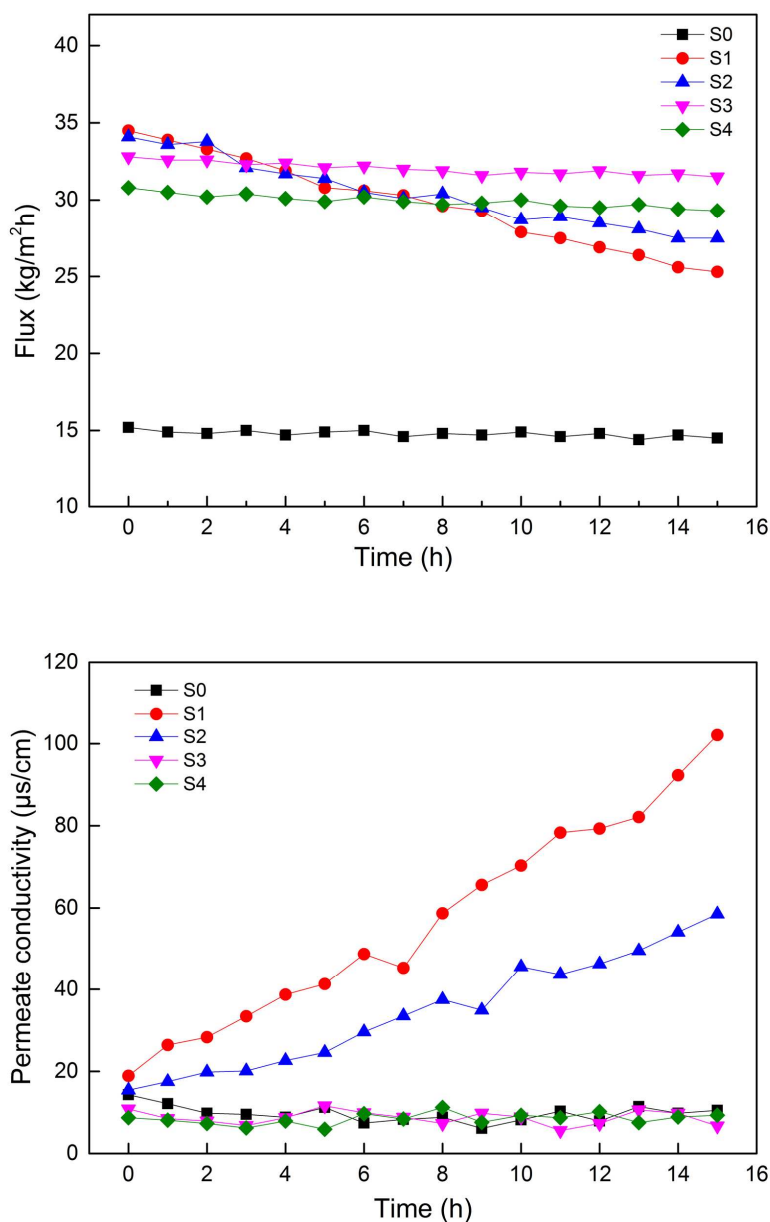
Fig. 9 Continuous VMD tests of FAS-PVDF-SiO$_2$ nanofiber membranes (S1-S4) and commercial PTFE membrane (S0) with 3.5 wt % NaCl solution

It can also be noticed that the initial permeate fluxes of FAS-PVDF-SiO$_2$ nanofiber membranes decrease with the increase of silica addition. The addition of SiO$_2$ decreases the porosity and mean pore size of the nanofiber membranes (Table 4), which mainly accounts for the slight decrease of the permeate flux. However, the fluxes of the FAS-PVDF-SiO$_2$ nanofiber membranes S1-S2 decreased gradually over the entire 15 hour test, indicating the occurrence of membrane wetting. This wetting issue was further evidenced by the test of

permeate conductivity, the permeate conductivities of S1 and S2 suffered a sharp increase over the entire test as shown in Fig. 9. On the contrary, the superhydrophobic FAS-PVDF-SiO$_2$ nanofiber membranes S3-S4 presented a stable permeate flux around 30 kg/m^{2}h and a low permeate conductivity approximately 10 μs/cm over the 15 h test. This phenomenon is consistent with the contact angle and LEPw tests as showed previously. Compared with membranes S3-S4, membranes S1-S2 possessed relatively lower LEPw values (< 120 kPa), thus making it susceptible to membrane wetting. The water molecules easily penetrated into the membrane pores and therefore decreased the permeability and increased the permeate conductivity of the nanofiber membranes [9]. Furthermore, the superhydrophobicity of membranes S3-S4 creates ample air pockets on the surface and makes the water drops easily rolls off, which could prevent the wetting of pores efficiently.

The VMD test results show that the nanofiber membranes exhibit higher permeate fluxes than commercial PTFE membrane owing to their higher porosities and inter-connected structures. Besides, the FAS modified nanofiber membranes S3-S4 with superhydrophobicity demonstrate a desirable anti-wetting performance during the long-stage test while S1-S2 suffered pore wetting, which is mainly ascribed to their high LEPw values and self-cleaning properties. The optimal FAS-PVDF-SiO$_2$ nanofiber membrane S3 presents a stable flux of about 31.5 kg/m^{2}h with satisfied conductivity over the entire test, indicating its great potentials in MD application.

4. Conclusions

Superhydrophobic FAS-PVDF-SiO$_2$ nanofiber membranes with high water contact angles and low contact angle hysteresis were successfully prepared via electrospinning of PVDF-SiO$_2$ blend solutions followed by a fluorosilanization process with FAS. The FAS modified nanofiber membranes achieved a liquid entry pressure of water (LEPw) as high as 195 kPa, while the LEPw of the pristine PVDF nanofiber membranes was only 84 kPa. The effect of SiO$_2$ addition on the properties of the FAS-PVDF-SiO$_2$ nanofiber membranes was also investigated. When the SiO$_2$ content increased in the dope solution, the fiber diameters and pore sizes of the nanofiber membranes decreased slightly, while the mechanical properties

were enhanced.

Continuous VMD experiments were carried out to test the anti-wetting performance of the FAS-PVDF-SiO$_2$ nanofiber membranes. The optimal superhydrophobic modified nanofiber membranes maintained a stable flux of about 31.5 kg/m^{2}h with a permeate conductivity approximately 10 µs/cm over the entire test, while the flux and conductivity of the nanofiber membranes without superhydrophobicity showed a significant decrease and increase, respectively. The results indicate that the newly developed FAS-PVDF-SiO$_2$ nanofiber membranes with high permeate flux and anti-wetting properties have great potential in vacuum membrane distillation for desalination.

Acknowledgements

References

[1]. T. Y. Cath, V. D. Adams and A. E. Childress, *J. Membr. Sci. ,* 2004, **228**, 5–16.

[2]. M. Gryta, M. Tomaszewska, J. Grzechulska and A. W. Morawski, *J. Membr. Sci.*, 2001, **181**, 279–287.

[3]. N. M. Mokhtar, W. J. Lau, A. F. Ismail, W. Youravong, W. Khongnakorn and K. Lertwittayanon, *RSC Adv.*, 2015, **5**, 38011.

[4]. B. W. Zhang, L. X. Liu, S. Y. Xie, F. Shen, H. Yan, H. H. Wu, Y. H. Wan, M. Yu, H. J. Ma, L. F. Li and J. Y. Li, *RSC Adv.*, 2014, **4**, 16561.

[5]. R. W. Schofield, A. G. Fane and C. J. D. Fell, *J. Membr. Sci.*, 1987, **33**, 299.

[6].   M. Khayet, J. I. Mengual and T. Matsuura, *J. Membr. Sci.*, 2005, **252**, 101.

[7].   C. Feng, K. C. Khulbe, T. Matsuura, R. Gopal, S. Kaur, S. Ramakrishna and M. Khayet, *J. Membr. Sci.*, 2008, **311**, 1–6.

[8].   L. D. Leonard, Y. C. Woo, M. A. H. Joir, J.-S. Choi and H. K. Shon, *Chem. Eng. J.*, 2014, **256**, 155–159.

[9].   Y. Liao, R. Wang, M. Tian, C. Q. Qiu and A. G. Fane, *J. Membr. Sci.*, 2013, **425-426**, 30–39.

[10].   J. A. Prince, G. Singha, D. Rana, T. Matsuura, V. Anbharasi and T. S. Shanmugasundaram, *J. Membr. Sci.*, 2012, **397-398**, 80–86.

[11].   M. Gryta and M. Barancewicz, *J. Membr. Sci.,* 2010, **358**, 158–167.

[12].   M. L. Ma and R. M. Hill, *Curr. Opin. Colloid Interface Sci.*, 2006, **11**, 193–202.

[13].   A. Lafuma and D. Quere, *Nat. Mater.*, 2003, **2**, 457–460.

[14].   Z. Ma, Y. Hong, L. Ma and M. Su, *Langmuir*, 2009, **25**, 5446–5450.

[15].   H. X. Wang, J. Fang, T. Cheng, J. Ding, L. T. Qu and L. M. Dai, *Chem. Commun.*, 2008, 877–879.

[16].   M. Manca, A. Cannavale, L. D. Marco, A. S. Arico, R. Cingolani and G. Gigli, *Langmuir*, 2009, **25 (11)**, 6357–6362.

[17].   S. S. Latthe, H. Imai, V. Ganesan and A. V. Rao, *Microporous Mesoporous Mater.*, 2010, **130**, 15–121.

[18].   J. Fresnais, J. P. Chapel and F. P. Epaillard, *Surf. Coat. Technol.*, 2006, **200**, 5296–5305.

[19].   S. Rezaei, I. Manoucheri, R. Moradian and B, Pourabbas, *Chem. Eng. J.*, 2014, **252**, 11–16.

[20].   Y. Zhang, Q. Zhang, C. F. Wang and S. Chen, *Ind. Eng. Chem. Res.*, 2013, **52**, 11590–11596.

[21].   L. Jiang, Y. Zhao and J. Zhai, *Angew. Chem. Int. Ed.*, 2004, **43**, 4338–4341.

[22].   M. L. Ma, R. M. Hill, J. L. Lowery, S. V. Fridrikh and G. C. Rutledge, *Langmuir*, 2005, **21**, 5549–5554.

[23].   M. H. Sun, C. X. Luo, L. P. Xu, H. Ji, Q. O. Yang, D. P. Yu and Y. Chen, *Langmuir*, 2005, **21**, 8978–8981.

[24].   H. Yabu, M. Takebayashi, M. Tanaka and M. Shimomura, *Langmuir*, 2005, **21**,

3235–3237.

[25]. J. Zhang, Z. Y. Song, B. A. Li, Q. Wang and S. C. Wang, *Desalination*, 2013, **324**, 1–9.

[26]. B. J. Privett, J. Youn, S. A. Hong, J. Lee, J. Han, J. H. Shin and M. H. Schoenfisch, *Langmuir*, 2011, **27**, 9597–9601.

[27]. R. Amir, E. Arifin, G. X. Dong, J. Mansouri and V. Chen, *J. Membr. Sci.*, 2012, **415–416**, 850–863.

[28]. Y. J. Kim, C. Y. Ahn, M. B. Lee and M. S. Choi, *Mater. Chem. Phys.*, 2011, **127**, 137–142.

[29]. M. Yanilmaz, C, Chen and X. W. Zhang, *J. Polym. Sci., Part B: Polym.Phys.*, 2013, **51**, 1719–1726.

[30]. P. P. Lu, Z. L. Xu, H. Yang and Y. M. Wei, *ACS. Appl. Mater. Interfaces.*, 2012, **4**, 1716–1723.

[31]. P. P. Lu, Z. L. Xu, H. Yang and Y. M. Wei, *Ind. Eng. Chem. Res.*, 2012, **51**, 11348–11354.

[32]. Z. Q. Dong, X. H. Ma, Z. L. Xu, W. T. You and F. B. Li, *Desalination*, 2014, **347**, 175–183.

[33]. X. H. Hua, Z. Q. Dong, P. Y. Zhang, Q. F. Zhong and Z. L. Xu, *Mater. Lett.*, 2015, **156**, 58–61.

[34]. M. Liu, Y. M. Wei, Z. L. Xu, R. Q. Guo and L, B, Zhao, *J. Membr. Sci.*, 2013, **437**, 169–178.

[35]. R. N. Wenzel, *Ind. Eng. Chem. Res*, 1936, **28**, 988–994.

[36]. K. W. Lawson and D. R. Lloyd, *J. Membr. Sci.*, 1997, **124**, 1–25.

[37]. K. Smolders and A. C. M. Franken, *Desalination*, 1989, **72**, 249–262.

[38]. N. Gao, M. Li, W. Jing, Y. Fan and N. Xu, *J. Membr. Sci.*, 2011, **375**, 276–283.

[39]. S. Koonaphapdeelert and K. Li, *J. Membr. Sc*i., 2007, **291**, 70–76.

[40]. J. Stabik, *Int Polym Process.*, 2004, **19**, 350–355.

[41]. J. Z. Liang, *Polym Test.*, 2002, **21**, 927–931.

[42]. B. Bhushan and Y. C. Jung, *Prog. Mater Sci.*, 2011, **56**, 1–108.

[43]. C. Y. Lai, A. Groth, S. Gray and M. Duke, *Water. Res.*, 2014, **57**, 56–66.

[44]. C. Y. Lai, A. Groth, S. Gray and M. Duke, *J. Membr. Sci.*, 2014, **149**, 146–157.

[45]. C. Y. Lai, A. Groth and S. Gray, M. Duke, *Membranes.*, 2014, **4**, 55–78.